

Distributions of molecules in the circumnuclear disk and surrounding starburst ring in the Seyfert galaxy NGC 1068 observed with ALMA

Shuro TAKANO^{1,2}, Taku NAKAJIMA³, Kotaro KOHNO^{4,5}, Nanase HARADA⁶, Eric HERBST⁷,
Yoichi TAMURA⁴, Takuma IZUMI⁴, Akio TANIGUCHI⁴, and Tomoka TOSAKI⁸

¹*Nobeyama Radio Observatory, Nobeyama, Minamimaki, Minamisaku, Nagano 384-1305*
takano.shuro@nao.ac.jp

²*Department of Astronomical Science, The Graduate University for Advanced Studies (Sokendai),*
Nobeyama, Minamimaki, Minamisaku, Nagano 384-1305

³*The Solar-Terrestrial Environment Laboratory, Nagoya University, Furo-cho, Chikusa-ku, Nagoya*
464-8601

⁴*Institute of Astronomy, University of Tokyo, 2-21-1 Osawa, Mitaka, Tokyo 181-0015*

⁵*Research Center for Early Universe, School of Science, The University of Tokyo, Hongo, Bunkyo,*
Tokyo 113-0033

⁶*Max-Planck-Institut für Radioastronomie, Auf dem Hügel 69, D-53121 Bonn, Germany*

⁷*Department of Chemistry, University of Virginia, McCormick Road, PO Box 400319,*
Charlottesville, VA 22904, USA

⁸*Joetsu University of Education, Yamayashiki-machi, Joetsu, Niigata 943-8512*

(Received ; accepted)

Abstract

Sensitive observations with the Atacama Large Millimeter/submillimeter Array (ALMA) allow astronomers to observe and discuss the detailed distributions of molecules with relatively weak intensity in nearby galaxies. In particular, we report distributions of several molecular transitions including shock and dust related species ($^{13}\text{CO } J = 1-0$, $\text{C}^{18}\text{O } J = 1-0$, $^{13}\text{CN } N = 1-0$, $\text{CS } J = 2-1$, $\text{SO } J_N = 3_2-2_1$, $\text{HNCO } J_{K_a, K_c} = 5_{0,5}-4_{0,4}$, $\text{HC}_3\text{N } J = 11-10, 12-11$, $\text{CH}_3\text{OH } J_K = 2_K-1_K$, and $\text{CH}_3\text{CN } J_K = 6_K-5_K$) in the nearby Seyfert 2 galaxy NGC 1068. This is the first paper reporting our study of molecular distributions in NGC 1068 with the ALMA early science program. The central ~ 1 arcmin (~ 4.3 kpc) of this galaxy was observed in the 100 GHz region (band 3) covering $\sim 96-100$ GHz and $\sim 108-111$ GHz with an angular resolution of $\sim 4'' \times 2''$ (290 pc \times 140 pc). These observations were motivated to study the effects of an active galactic nucleus and its surrounding starburst ring on molecular abundances. In this article, we present images and report a classification of

molecular distributions into three main categories, defined as follows: (1) Molecules concentrated in the circumnuclear disk (CND) (SO $J_N = 3_2-2_1$, HC₃N $J = 11-10$, $12-11$, and CH₃CN $J_K = 6_K-5_K$), (2) Molecules distributed both in the CND and the starburst ring (CS $J = 2-1$ and CH₃OH $J_K = 2_K-1_K$), (3) Molecules distributed mainly in the starburst ring (¹³CO $J = 1-0$ and C¹⁸O $J = 1-0$). Since most of the molecules such as HC₃N observed in the CND are easily dissociated by UV photons and X-rays, our results indicate that these molecules must be effectively shielded. In the starburst ring, the distribution of CH₃OH is similar to those of ¹³CO, C¹⁸O, and CS on the whole, but the relative intensity of methanol at each clumpy region is not consistent with those of ¹³CO, C¹⁸O, and CS. This difference is probably caused by the unique formation and destruction mechanisms of CH₃OH in the environment of the starburst ring.

Key words: line: identification — galaxies: individual (NGC 1068) — galaxies: Seyfert — galaxies: starburst — radio lines: galaxies

1. Introduction

Recent rapid advances in millimeter/submillimeter (mm/submm) receivers equipped with wide-band spectroscopic capabilities, such as EMIR with the WILMA spectrometer on the IRAM 30m telescope (Carter et al. 2012), Z-Spec on the CSO 10.4m telescope (Bradford et al. 2004), Redshift-search-receiver on the LMT 50m (Erickson et al. 2007), TZ with the SAM45 spectrometer on the NRO 45m telescope (Iono et al. 2012; Nakajima et al. 2013), and SPIRE-FTS on Herschel (Griffin et al. 2010), have revolutionalized our view concerning chemical properties in galaxies. Unbiased spectral line surveys toward various types of galaxies have been conducted (e.g., Martín et al. 2006; Naylor et al. 2010; van der Werf et al. 2010; Snell et al. 2011; Costagliola et al. 2011; Nakajima et al. 2011; Martín et al. 2011; Kamenetzky et al. 2011; Rangwala et al. 2011; Aladro et al. 2011, 2013), revealing the richness and diversity of spectral line features.

These chemical properties have been expected to be powerful astrophysical tools for the study of galaxies, because activity in the central regions of galaxies, such as a burst of massive star-formation or an active galactic nucleus (AGN), must have a strong impact on the chemical and physical properties of the surrounding interstellar medium (ISM). For instance, elevated HCN emission with respect to CO and/or HCO⁺ has often been detected toward AGNs (e.g., Jackson et al. 1993; Tacconi et al. 1994; Helfer & Blitz 1995; Kohno et al. 1996, 2003; Krips et al. 2007, 2008; Krips 2012; Izumi et al. 2013), where it is expected to be the imprint of either strong X-ray irradiation/ionization (Usero et al. 2004; García-Burillo et al. 2010; Davies et al. 2012) and/or a high-temperature environment caused by AGN activity (e.g., Harada et al. 2010; Izumi et al. 2013). Nevertheless, some controversial observational results (e.g., Baan

et al. 2008; Snell et al. 2011; Costagliola et al. 2011; Sani et al. 2012) and theoretical work on the physical and chemical properties of the ISM in external galaxies (e.g., Meijerink & Spaans 2005; Meijerink et al. 2007), which are somewhat inconsistent with the idea of the enhanced HCN emission among AGNs, suggest that our current understanding of physical and chemical properties in galaxies is still far from complete.

One of the promising directions for study is to build detailed inventories of spectral lines in the vicinity of AGNs. By comparing them with the results of spectral line surveys in the central regions of starburst galaxies such as NGC 253 (e.g., Martín et al. 2006) and M82 (e.g., Aladro et al. 2011), we can identify the key combinations of molecules that differentiate the power sources in galaxies. For this purpose, the circumnuclear disk (CND; Usero et al. 2004) of NGC 1068 is one of the best targets, although NGC 1068 is known to host intense starburst regions along the inner spiral arms or ring (e.g., Telesco & Decher 1988). Since the diameter of the starburst ring is fairly large ($\sim 30''$), the emission from the CND ($< 4''$) can be easily separated spatially, if we employ mm/submm interferometers. Note that little if any signature for recent nuclear starburst activity has been identified in the central region of NGC 1068 (e.g., Imanishi et al. 1997; Cid Fernandes et al. 2001; Davies et al. 2007), despite the fact that the CND is bright in CO and other molecular lines (e.g., Schinnerer et al. 2000; Tsai et al. 2012). This makes the CND of NGC 1068 ideal for the study of the AGN imprints, because nuclear starbursts often cohabit with AGNs (e.g., Imanishi & Wada 2004), hampering clear separation of spectral line features between starbursts and AGNs.

To date, several unbiased line survey works at mm/submm wavelengths have been reported towards the center of NGC 1068 (Snell et al. 2011; Costagliola et al. 2011; Kamenetzky et al. 2011; Spinoglio et al. 2012; Aladro et al. 2013) using single dish telescopes, but contamination from starbursts associated with inner spiral arms/ring could be a problem if we consider the sizes of the observing beams ($14''$ – $70''$). On the other hand, interferometric imaging of the CND give clean measurements of spectral lines, but the observed lines are limited to major species such as CO, HCN, HCO⁺, CS, CN, and SiO (e.g., Papadopoulos et al. 1996; Tacconi et al. 1997; Kohno et al. 2008; García-Burillo et al. 2010; Krips et al. 2011) due to the limitation in sensitivity of the existing pre-ALMA mm/submm arrays.

In this situation, we proposed to observe several interesting molecules simultaneously in the 98 and 110 GHz regions sensitively with ALMA. These frequency regions are rich in molecules, including typical shock/dust related species and the CO isotopologues. We first obtained the intensities of such lines based on our line survey project with the 45m telescope (Nakajima et al. 2011). As an additional advantage of this frequency region, the primary beams of the ALMA 12m antennas (~ 1 arcmin) cover both the CND and the starburst ring in one field of view, which is useful for our purposes.

In this paper, we report a high-resolution imaging study of molecular lines in the central region (~ 1 arcmin) of NGC 1068 observed with ALMA. Even in its early science operation

phase, ALMA is already powerful enough to simultaneously observe 10 lines from 9 molecules ($^{13}\text{CO } J = 1-0$, $\text{C}^{18}\text{O } J = 1-0$, $^{13}\text{CN } N = 1-0$, $\text{CS } J = 2-1$, $\text{SO } J_N = 3_2-2_1$, $\text{HNC O } J_{K_a, K_c} = 5_{0,5}-4_{0,4}$, $\text{HC}_3\text{N } J = 11-10, 12-11$, $\text{CH}_3\text{OH } J_K = 2_K-1_K$, and $\text{CH}_3\text{CN } J_K = 6_K-5_K$) within a frequency coverage of ~ 7.0 GHz at the 3 mm band, uncovering a wide variety of molecular line distributions. We describe our observations and data reduction in Section 2, and present the images and spectra of the observed molecular lines in Section 3. In Section 4, the molecular distributions will be classified into three main categories: (1) Molecules concentrated in the CND, (2) Molecules distributed both in the CND and the starburst ring, and (3) Molecules distributed mainly in the starburst ring. Some implications of this diversity are also discussed in this section. Throughout the paper, we assume that the distance of NGC 1068 is 14.4 Mpc (Tully 1988; Bland-Hawthorn et al. 1997); at this distance, $1''$ corresponds to 72 pc.

2. Observations and data reduction

The observations were carried out with ALMA in the early science program (cycle 0) in January 2012. The receivers in band 3 (100 GHz region) were used. The 16 antennas available were in the compact configuration. The adopted central position of NGC 1068 was $\text{RA}(\text{J2000.0}) = 2^{\text{h}}42^{\text{m}}40^{\text{s}}.798$ and $\text{Dec}(\text{J2000.0}) = -00^{\circ}00'47''.938$. The systemic velocity employed was 1150 km s^{-1} . The position and the velocity were taken from Schinnerer et al. (2000). This position is the radio core at the AGN observed with MERLIN (The Multi-Element Radio Linked Interferometer Network) at 5 GHz (Muxlow et al. 1996).

As a correlator setup, the two spectral windows were placed in the lower sideband (LSB: covering $\sim 96-100$ GHz), and the other two were placed in the upper sideband (USB: covering $\sim 108-111$ GHz). Each spectral window covered 1875 MHz with 3840 channels resulting in a frequency resolution of 488 kHz. Such a setup efficiently covered frequency regions with rich spectral lines, as mentioned in the Introduction. The final results were presented with the velocity resolution of $\sim 19 \text{ km s}^{-1}$ (at 100 GHz) to improve the signal-to-noise ratio.

The total observational time was about 110 minutes including calibration and overheads. The spatial resolution of the observations was $4''2 \times 2''4$ ($\sim 300 \text{ pc} \times 170 \text{ pc}$) at the principal axis of 176 deg in the spectral window of the lowest frequency. The system temperature was $\sim 53-133$ K depending on frequency and antennas. The achieved noise level (rms) was $\sim 1.1-1.7 \text{ mJy beam}^{-1}$ depending on the spectral window and image region. The observational parameters are summarized in Table 1.

The data were reduced with the reduction software CASA (mainly with ver. 3.4). We used continuum subtracted calibrated data (measurement set) and image cubes provided by the ALMA Regional Center. For molecular lines with no provided image cubes (^{13}CN , HNC O , and CH_3CN), we obtained images from the measurement set above. The images of integrated intensity (moment 0 maps) were made using pixels with all flux values in the image cubes.

3. Results

3.1. Overview of the images

Thanks to the high sensitivity of ALMA, all expected lines were detected with a short observational time. The integrated intensity images are shown in Figures 1 and 2. In Figure 1 images with a significant distribution in the starburst ring are shown. These images are from the $^{13}\text{CO } J = 1-0$, $\text{C}^{18}\text{O } J = 1-0$, $\text{CS } J = 2-1$, and $\text{CH}_3\text{OH } J_K = 2_K-1_K$ rotational transitions.

- ^{13}CO and C^{18}O : The images of these CO isotopic species show rather weak signals in the CND, but show clear distributions in the starburst ring. In particular, a southwest region in the starburst ring shows the strongest emission. These overall pictures agree well with the past interferometric $^{13}\text{CO } (J = 1-0)$ images (e.g., Helfer & Blitz 1995; Papadopoulos et al. 1996; Tacconi et al. 1997), but the quality of the image is greatly improved with ALMA. The clear distributions in the starburst ring are also qualitatively similar to those of the $^{12}\text{CO } J = 1-0$ and $3-2$ transitions (e.g., Schinnerer et al. 2000; Tsai et al. 2012), but the emission in the CND is clearly seen in these ^{12}CO images. The difference in the emission in the CND between ^{12}CO and our CO isotopic species indicates that the CO $J = 1-0$ emission in the CND is optically thinner than that in the starburst ring. A quantitative analysis will be done with the ALMA band 7 data (~ 330 GHz region) by Nakajima et al. (in preparation) and Taniguchi et al. (in preparation). Next, the total flux ratio of the CO isotopic species ($\text{C}^{18}\text{O}/^{13}\text{CO}$) was calculated, and the obtained value is ~ 0.34 . This ratio is similar to the corresponding ratio of 0.3 from past interferometric data using the OVRO (Owens Valley Radio Observatory) mm-array (Papadopoulos et al. 1996) and the value of 0.28 calculated from line survey data with the IRAM 30m telescope (Aladro et al. 2013). In addition, we are investigating the properties of giant molecular associations based on the ^{13}CO , C^{18}O , CS, and CH_3OH lines with data cubes of high spectral resolution produced from the same data of band 3. The relation to the star-formation rate (SFR) is also being investigated. The results will be published separately (Tosaki et al., in preparation).
- CS: The strong emission is concentrated in the CND, while weak emission is seen in the starburst ring. This is in sharp contrast to the distributions of the CO isotopic species. Since CS is a typical high-density tracer, the CS distributed area should have a relatively high density in the first order approximation. In the starburst ring, the CS emission is relatively strong in the southwestern region. This pattern is the same as the distributions of the CO isotopic species in the starburst ring. A CS $J = 2-1$ image was also reported by Tacconi et al. (1997); these authors used the IRAM Plateau de Bure interferometer. Their results also show the central concentration and additional clumpy features in the starburst ring.
- CH_3OH : Our data yield the first interferometric image in NGC 1068. Methanol is distributed both in the CND and in the starburst ring with similar intensity. Although the

signal-to-noise ratio is not high enough, methanol is probably distributed both in the east and west knots (Schinnerer et al. 2000) in the CND. The distribution in the starburst ring is similar to those of ^{13}CO , C^{18}O , and CS on the whole, but the relative intensity of methanol at each clumpy region is not as consistent with those of ^{13}CO , C^{18}O , and CS. In particular, a striking difference can be seen in the eastern region, where methanol emission is the strongest, although the intensities of the CO isotopic species and CS are relatively weak. Methanol is thought to be produced on grain surfaces (e.g., Watanabe & Kouchi 2002) and sublimed into the gas-phase by star-formation activities. This interesting distribution of methanol and its relation to star formation will be discussed later.

In Figure 2, images exhibiting concentrated distributions in the CND are shown. These images involve rotational lines of the following transitions: $^{13}\text{CN } N = 1-0$, $\text{SO } J_N = 3_2-2_1$, $\text{HNCO } J_{K_a, K_c} = 5_{0,5}-4_{0,4}$, $\text{HC}_3\text{N } J = 11-10, 12-11$, and $\text{CH}_3\text{CN } J_K = 6_K-5_K$, and are the first interferometric images for the rotational lines in NGC 1068.

- ^{13}CN : The image was made using two fine structure lines ($J = 3/2-1/2$ and $1/2-1/2$) of the $N = 1-0$ transition. Although the signal-to-noise ratio is low, ^{13}CN may be distributed both in the east and west knots in the CND. It is not clear whether ^{13}CN is distributed in the starburst ring, because the clumpy ring-like structure looks different from those of the CO isotopic species and CH_3OH . Previously, the CN $N = 2-1$ image was reported by García-Burillo et al. (2010), who used the IRAM Plateau de Bure interferometer. Their results show distributions both in the east and west knots in the CND; the intensity is stronger in the east knot than in the west knot. These facts support our results for ^{13}CN in the CND. Since their field of view is $21''$, the image does not cover the starburst ring.
- SO: The image is concentrated in the CND.
- HNCO: Although the signal-to-noise ratio is low, HNCO may be distributed both in the east and west knots in the CND, and is distributed in the starburst ring, though it is not clearly seen in the image. As shown later, the distribution of HNCO in the starburst ring is confirmed from the detection of its spectral line in the southwest point of the starburst ring.
- HC_3N : The image is concentrated in the CND as seen from two rotational emission lines.
- CH_3CN : The image is concentrated in the CND.

3.2. Spectra at the circumnuclear disk and the starburst ring (southwest)

Spectra were obtained from cleaned images at the following two positions:

- (1) The central radio continuum peak (AGN) in the CND ($\text{RA}(\text{J2000.0}) = 2^{\text{h}}42^{\text{m}}40^{\text{s}}70912$ and $\text{Dec}(\text{J2000.0}) = -00^{\circ}00'47''9449$, Gallimore et al. 2004)
- (2) The $^{13}\text{CO } J = 3-2$ intensity peak at the southwest position in the starburst ring ($\text{RA}(\text{J2000.0}) = 2^{\text{h}}42^{\text{m}}40^{\text{s}}298$ and $\text{Dec}(\text{J2000.0}) = -00^{\circ}01'01''638$, Nakajima et al. in preparation).

Before obtaining the spectra, the images in the two spectral windows in the USB were convolved with the beam of the spectral window in the lowest frequency in the LSB, and then, attenuation due to the primary beam pattern of the ALMA 12m antennas was corrected. The velocity resolution is $\sim 19.0 \text{ km s}^{-1}$ at 100 GHz. The obtained spectra are shown in Figure 3.

In the CND, the detected lines are broad, with a width of about 200 km s^{-1} FWHM. C^{18}O is not clearly detected, and ^{13}CN is marginally detected in the CND. On the other hand, the detected lines in the southwest position of the starburst ring are narrow with a width of about $20\text{--}45 \text{ km s}^{-1}$ FWHM. Detections of $\text{SO } J_N = 3_2\text{--}2_1$, $\text{HC}_3\text{N } J = 11\text{--}10, 12\text{--}11$, and $\text{HNCO } J_{K_a, K_c} = 5_{0,5}\text{--}4_{0,4}$ clearly indicate the existence of such molecules there, which is not unambiguously determined by the images in figure 2. The $\text{CH}_3\text{CN } J_K = 6_K\text{--}5_K$ transition is not detected. The detected lines were Gaussian fitted, and the line parameters obtained are summarized in Table 2.

3.3. Total flux and the flux at the circumnuclear disk

As presented in Figures 1 and 2, the distributions of molecules show wide diversity. In order to obtain quantitative information of the distributions, we extracted both the total flux and the flux in the CND for each molecule. The derived flux ratio (CND/Total) was then used to determine a general trend.

The total flux was obtained from the images within a circle of $55''$ diameter, which covers both the CND and the starburst ring. The flux in the CND is obtained within a circle of $10''$ diameter. Both of the circles are centered on the radio continuum peak (Gallimore et al. 2004). The results are listed in Table 3. The error for each flux is obtained from the standard deviation of the pixel values of the image, but the systematic deviation is not included. For images with low signal-to-noise ratio, it is difficult to obtain a reliable total flux from the relatively wide area of the $55''$ diameter, because the effect of systematic deviation in the image can be significant. In such a case, the obtained values were not presented in this table. We also note that the accuracy of the ^{13}CO flux in the CND may be limited by the dynamic range of the data (Taniguchi et al., in preparation), because the emission from the CND is surrounded by much stronger sources of emission along the starburst ring.

The value of the flux ratio, which is presented in Table 3, ranges widely from 0.006 to more than 0.7. By comparing the ratio and the image, we can approximately establish the correspondence between the ratio and the distribution as follows:

- (1) 0.7–1.0 for molecules concentrated in the CND,
- (2) 0.1–0.4 for molecules distributed both in the CND and the starburst ring,
- (3) 0.0–0.02 for molecules distributed mainly in the starburst ring.

The flux ratio is also presented in Figure 4.

3.4. Comparison of flux with single dish telescopes

We compared the flux obtained from ALMA with those from single dish telescopes (NRO 45m and IRAM 30m) to estimate the recovery of the flux with the interferometer. First, the flux of ^{13}CO was compared. The image obtained with ALMA, with the primary beam corrected, was convolved with the 45m beam of $16''$, and the flux obtained was converted to a brightness temperature of $\sim 8.1 \text{ K km s}^{-1}$. The corresponding value obtained with the 45m telescope is $\sim 8.9 \text{ K km s}^{-1}$, which was observed in the recent line survey project (Nakajima et al. and Takano et al., in preparation). Therefore, the recovered flux is about 92 %. The same comparison was carried out by convolving the ALMA data with the 30m beam of $22''$, and the flux obtained was once again converted to brightness temperature, this time $\sim 10.1 \text{ K km s}^{-1}$. The corresponding value obtained with the 30m telescope is $\sim 12.8 \text{ K km s}^{-1}$ (Aladro et al. 2013), so that the recovered flux is about 79 %. The 30m telescope can observe widely distributed gas more efficiently than the 45m telescope due to the larger beam size, but ALMA is less sensitive to such gas. The difference in the values of the recovery may include such an effect.

Second, the flux of CS, which is more compactly distributed than ^{13}CO , was compared. The image obtained with ALMA, with primary beam corrected, was convolved with the 45m beam of $17''$, and the flux obtained was converted to a brightness temperature of $\sim 5.9 \text{ K km s}^{-1}$. The corresponding value obtained with the 45m telescope is $\sim 8.0 \text{ K km s}^{-1}$ (Nakajima et al. and Takano et al., in preparation). Therefore, the recovered flux is about 74 %. The comparison with the CS data of the 30m telescope was not done, because the line is blended with a line from the other sideband (Aladro et al. 2013). These results of ^{13}CO and CS indicate that ALMA observes a significant amount of gas in the central region of NGC 1068.

4. Discussion

4.1. Classification of molecular distributions

As presented in Figures 1 and 2, the molecules exhibit a wide variety of distributions, which are reflections of abundance and excitation. Such distributions contain important information to study the effects on molecules caused by AGN activity and starburst conditions. As already mentioned in the previous sections, we can classify molecular distributions into three broad categories:

- (1) Molecules concentrated in the CND,
- (2) Molecules distributed both in the CND and the starburst ring,
- (3) Molecules distributed mainly in the starburst ring.

Based in addition on the spectra shown in Figure 3 and on the flux ratio (CND/Total) in Table 3, each molecule was further classified as listed in Table 4, where the above categories (1) and (2) were subdivided as follows:

- Molecules distributed in two knots in the CND,
- Molecules distributed in the center of the CND.

Higher spatial resolution and better signal-to-noise ratio are desirable for this more precise classification, but indications of such differences can be seen in the present images. In Table 4, the refined classification of HCN ($J = 1-0$), HCO⁺ ($J = 1-0$), and SiO ($J = 2-1$) is also included based on their images in the literature (e.g., Jackson et al. 1993; Kohno et al. 2008; García-Burillo et al. 2010). Distributions of ¹³CO, C¹⁸O, CN, and CS obtained from our ALMA band 7 data (Nakajima et al. in preparation) are also included.

4.2. Implications for molecular formation and destruction mechanisms

We discuss the implications of specific molecular distributions below using a knowledge of the relevant reactions and the results of model calculations. Further discussion will be undertaken after we obtain quantitative information such as the abundances in Nakajima et al. (in preparation). Here we mainly use the results of recent models by Harada et al. (2010, 2013) and Aladro et al. (2013). Harada et al. (2010) reported a gas-phase time-dependent reaction model including reactions with significant activation energies for high-temperature chemistry. Thus, this model can be used for high-temperature sources up to ~ 800 K. Harada et al. (2013) applied the results of Harada et al. (2010) to the axisymmetric accretion disk around AGNs such as that in NGC 1068. The effects of X-rays and cosmic rays are included. Aladro et al. (2013) reported a time-dependent reaction model including gas-phase and grain surface reactions. The effects of UV photons and cosmic rays are included. A high cosmic ray ionization rate was used to simulate the environment in an X-ray dissociation region (XDR).

4.2.1. HC₃N

Because HC₃N is concentrated in the CND, its behavior cannot be explained if we consider the entire CND as an XDR, since HC₃N is easily dissociated by cosmic rays and UV photons (Aladro et al. 2013; Harada et al. 2013). On the other hand, the abundance of HC₃N increases at hot core regions and high-temperature (non-dissociative shocked) regions (Caselli et al. 1993; Harada et al. 2010). The model by Harada et al. (2013) shows that there is a high-temperature midplane where X-rays cannot penetrate into the CND in addition to a different layer that can be characterized as an XDR. Complex molecules are predicted to be abundant in the high temperature zone. Our observations of HC₃N confirm that there is a large amount of gas which is shielded from X-rays, and the local column densities of the CND should be very high. This fact yields information on the structure of the CND, which is quite interesting and relevant to an understanding of the physical and chemical environment in the central region. Further ALMA observations with higher angular resolution will reveal the structure.

4.2.2. CH₃OH

Methanol has a significant concentration in the CND as mentioned before. Just like HC₃N, methanol is easily dissociated by cosmic rays and UV photons (Aladro et al. 2013).

Thus, the concentration of methanol in the CNB also requires shielding. On the other hand, the inconsistent distribution of methanol in the starburst ring is very striking. The formation of methanol on icy dust grains is well known and it is not surprising that methanol should be abundant in active star-forming regions in the starburst ring.

To look at the matter further, we studied the relation of methanol intensity to the star-formation rate (SFR, Tsai et al. 2012) in those regions with relatively strong methanol emission. We found the averaged SFR in regions with relatively strong methanol emission (roughly at regions R6, R9, R16, and R20–21 in Tsai et al. (2012)) to be $1.40 \pm 0.54 M_{\odot} \text{ yr}^{-1} \text{ kpc}^{-2}$, whereas the average of all regions is $1.26 \pm 0.46 M_{\odot} \text{ yr}^{-1} \text{ kpc}^{-2}$. The averaged value of regions with relatively strong methanol emission is only slightly larger than that of all the regions. Moreover, the values at regions with relatively strong methanol emission have a large scatter from 0.97 to $2.26 M_{\odot} \text{ yr}^{-1} \text{ kpc}^{-2}$ (Tsai et al. 2012) as indicated in the large standard deviation. Thus, we could not find a strong correlation between methanol intensity and the SFR. This result may be related to our spatial resolution and its coupling to the sizes of the regions above, or this may be due to the formation and destruction mechanisms in the environment of the starburst ring. A more detailed analysis will be published separately (Tosaki et al. in preparation).

The inconsistent distribution of CH_3OH in the starburst ring when compared with ^{13}CO and/or C^{18}O , discussed here, was also reported in IC 342 (Meier & Turner 2005) and Maffei 2 (Meier & Turner 2012). In addition, CH_3OH is relatively weak in M82 (e.g., Aladro et al. 2011), which is in a late stage of starburst activity. These presumably related results should be very helpful in interpreting the inconsistency in the starburst ring in NGC 1068, suggesting that methanol needs specific favorable conditions to form on grains and to subsequently sublime into the gas phase.

4.2.3. *SO, HNC, and CH_3CN*

Because they are concentrated in the CNB, the distributions of these molecules clearly indicate that the CNB is a good environment to maintain their abundances. SO and CH_3CN are easily dissociated by UV photons, but the abundance of SO is enhanced by cosmic rays (Aladro et al. 2013). Thus, the XDR environment seems to be a favorable place for SO , but the concentration of CH_3CN also suggests shielded gas in the CNB.

Similar to other molecules, HNC can also be dissociated by UV photons, and it needs to be shielded. Although there is a gas-phase production route for this molecule, its abundance is known to increase when HNC on dust surfaces sublimates (Quan et al. 2010).

The above mentioned molecules except CH_3CN (SO , HNC , HC_3N , and CH_3OH) are also detected in the southwest starburst ring. These facts do not contradict the detections of these molecules in other starburst galaxies such as NGC 253 and M82 (e.g., Martín et al. 2006; Aladro et al. 2011).

4.2.4. Two kinds of distributions in the CND

The molecules in the CND show two kinds of distributions as mentioned previously in subsection 4.1. Here we briefly discuss possible reasons for such a difference. Let us start with the case of SiO, which is distributed in the center, as observed by García-Burillo et al. (2010), who also reported an enhanced SiO abundance and discussed its likely shock origin. Probably SiO is produced through the sputtering of Si-bearing material in grains (Field et al. 1997; Caselli et al. 1997; Schilke et al. 1997), and as a result SiO traces strong shocks in the central region. On the other hand, HNC and CH₃OH are tracing relatively weak shocks, which result in the sublimation of HNC and CH₃OH from the icy mantles of dust grains (e.g., Rodríguez-Fernández et al. 2010; Bachiller et al. 1995). Therefore, it seems that molecules produced in more energetic regions tend to exist closer to the center, while those produced in less energetic regions exhibit a bipolar pattern in the knots.

As shown in this study, the sensitive ALMA observations are very powerful probes of the distributions of molecules in gas-rich nearby galaxies such as NGC 1068 even in the early operation phase of ALMA. Further observations of many other molecules will bring us additional valuable information to understand chemical processes in such environments.

5. Summary

We have observed the Seyfert 2 galaxy NGC 1068 in its central 1 arcmin at the 100 GHz frequency region during the ALMA early science program; our observations included both the CND and the starburst ring.

We observed the rotational transitions ¹³CO $J = 1-0$, C¹⁸O $J = 1-0$, ¹³CN $N = 1-0$, CS $J = 2-1$, SO $J_N = 3_2-2_1$, HNC $J_{Ka,Kc} = 5_{0,5}-4_{0,4}$, HC₃N $J = 11-10, 12-11$, CH₃OH $J_K = 2_K-1_K$, and CH₃CN $J_K = 6_K-5_K$. The molecular transitions show a wide variety of spatial distributions, which can be classified into three main categories: those molecular transitions concentrated in the CND, those distributed both in the CND and the starburst ring, and those mainly in the starburst ring. The distributions concentrated in the CND include ¹³CN, SO, HNC, HC₃N, and CH₃CN; those distributed in the CND and starburst ring include CS and CH₃OH, while those mainly in the starburst ring include ¹³CO and C¹⁸O. The first two categories were further subdivided into distributions in the two knots or in the center of the CND.

Molecules concentrated in the CND are easily dissociated by cosmic rays, X-rays, and/or UV photons. These facts indicate that there is a large amount of gas in the CND, which is shielded especially from X-rays. This information constrains the structure of the CND.

The distribution of methanol in the starburst ring shows an inconsistent relative intensity with respect to those of ¹³CO, C¹⁸O, and CS. In addition, the intensity of methanol does not seem to correlate with the star formation efficiency, although methanol is thought to be formed on grain surfaces and sublimated into the gas-phase by external heating.

This paper makes use of the ALMA data ADS/JAO.ALMA#2011.0.00061.S. ALMA is a partnership of ESO (representing its member states), NSF (USA) and NINS (Japan), together with NRC (Canada) and NSC and ASIAA (Taiwan), in cooperation with the Republic of Chile. The Joint ALMA Observatory is operated by ESO, AUI/NRAO and NAOJ. We thank the support of the East Asian ALMA Regional Center, in particular, A. Kawamura, for the support. S. T. thanks Y. Shimajiri, M. Oya, and S. Takahashi for the support of the analysis with CASA. E. H. wishes to acknowledge the support of the National Science Foundation for his astrochemistry program. He also acknowledges support from the NASA Exobiology and Evolutionary Biology program through a subcontract from Rensselaer Polytechnic Institute.

References

- Aladro, R., Martín, S., Martín-Pintado, J., Mauersberger, R., Henkel, C., Ocaña Flaquer, B., & Amo-Baladrón, M. A. 2011, *A&A*, 535, A84
- Aladro, R., et al. 2013, *A&A*, 549, A39
- Baan, W. A., Henkel, C., Loenen, A. F., Baudry, A., & Wiklind, T. 2008, *A&A*, 477, 747
- Bachiller, R., Liechti, S., Walmsley, C. M., & Colomer, F. 1995, *A&A*, 295, L51
- Bland-Hawthorn, J., Gallimore, J. F., Tacconi, L. J., Brinks, E., Baum, S. A., Antonucci, R. R. J., & Cecil, G. N. 1997, *Ap&SS*, 248, 9
- Bradford, C. M., et al. 2004, in *Society of Photo-Optical Instrumentation Engineers (SPIE) Conference Series*, Vol. 5498, *Society of Photo-Optical Instrumentation Engineers (SPIE) Conference Series*, ed. C. M. Bradford, P. A. R. Ade, J. E. Aguirre, J. J. Bock, M. Dragovan, L. Duband, L. Earle, J. Glenn, H. Matsuhara, B. J. Naylor, H. T. Nguyen, M. Yun, & J. Zmuidzinas, 257
- Carter, M., et al. 2012, *A&A*, 538, A89
- Caselli, P., Hartquist, T. W., & Havnes, O. 1997, *A&A*, 322, 296
- Caselli, P., Hasegawa, T. I., & Herbst, E. 1993, *ApJ*, 408, 548
- Cid Fernandes, R., Heckman, T., Schmitt, H., González Delgado, R. M., & Storchi-Bergmann, T. 2001, *ApJ*, 558, 81
- Costagliola, F., et al. 2011, *A&A*, 528, A30
- Davies, R., Mark, D., & Sternberg, A. 2012, *A&A*, 537, A133
- Davies, R. I., Müller Sánchez, F., Genzel, R., Tacconi, L. J., Hicks, E. K. S., Friedrich, S., & Sternberg, A. 2007, *ApJ*, 671, 1388
- Erickson, N., Narayanan, G., Goeller, R., & Grosslein, R. 2007, in *Astronomical Society of the Pacific Conference Series*, Vol. 375, *From Z-Machines to ALMA: (Sub)Millimeter Spectroscopy of Galaxies*, ed. A. J. Baker, J. Glenn, A. I. Harris, J. G. Mangum, & M. S. Yun, 71
- Field, D., May, P. W., Pineau des Forets, G., & Flower, D. R. 1997, *MNRAS*, 285, 839
- Gallimore, J. F., Baum, S. A., & O’Dea, C. P. 2004, *ApJ*, 613, 794
- García-Burillo, S., et al. 2010, *A&A*, 519, A2
- Griffin, M. J., et al. 2010, *A&A*, 518, L3
- Harada, N., Herbst, E., & Wakelam, V. 2010, *ApJ*, 721, 1570
- Harada, N., Thompson, T. A., & Herbst, E. 2013, *ApJ*, 765, 108
- Helfer, T. T. & Blitz, L. 1995, *ApJ*, 450, 90
- Imanishi, M., Terada, H., Sugiyama, K., Motohara, K., Goto, M., & Maihara, T. 1997, *PASJ*, 49, 69
- Imanishi, M. & Wada, K. 2004, *ApJ*, 617, 214
- Iono, D., et al. 2012, *PASJ*, 64, L2
- Izumi, T., et al. 2013, *PASJ*, 65, 100

Jackson, J. M., Paglione, T. A. D., Ishizuki, S., & Nguyen-Q-Rieu. 1993, *ApJL*, 418, L13

Kamenetzky, J., et al. 2011, *ApJ*, 731, 83

Kohno, K., Ishizuki, S., Matsushita, S., Vila-Vilaró, B., & Kawabe, R. 2003, *PASJ*, 55, L1

Kohno, K., Kawabe, R., Tosaki, T., & Okumura, S. K. 1996, *ApJL*, 461, L29+

Kohno, K., Nakanishi, K., Tosaki, T., Muraoka, K., Miura, R., Ezawa, H., & Kawabe, R. 2008, *Ap&SS*, 313, 279

Krips, M. 2012, *Journal of Physics Conference Series*, 372, 012038

Krips, M., et al. 2011, *ApJ*, 736, 37

Krips, M., et al. 2007, *A&A*, 468, L63

Krips, M., Neri, R., García-Burillo, S., Martín, S., Combes, F., Graciá-Carpio, J., & Eckart, A. 2008, *ApJ*, 677, 262

Lovas, F. J. 1992, *Journal of Physical and Chemical Reference Data*, 21, 181

Martín, S., et al. 2011, *A&A*, 527, A36

Martín, S., Mauersberger, R., Martín-Pintado, J., Henkel, C., & García-Burillo, S. 2006, *ApJS*, 164, 450

Meier, D. S. & Turner, J. L. 2005, *ApJ*, 618, 259

Meier, D. S. & Turner, J. L. 2012, *ApJ*, 755, 104

Meijerink, R. & Spaans, M. 2005, *A&A*, 436, 397

Meijerink, R., Spaans, M., & Israel, F. P. 2007, *A&A*, 461, 793

Muxlow, T. W. B., Pedlar, A., Holloway, A. J., Gallimore, J. F., & Antonucci, R. R. J. 1996, *MNRAS*, 278, 854

Nakajima, T., et al. 2013, *PASP*, 125, 252

Nakajima, T., Takano, S., Kohno, K., & Inoue, H. 2011, *ApJL*, 728, L38

Naylor, B. J., et al. 2010, *ApJ*, 722, 668

Papadopoulos, P. P., Seaquist, E. R., & Scoville, N. Z. 1996, *ApJ*, 465, 173

Quan, D., Herbst, E., Osamura, Y., & Roueff, E. 2010, *ApJ*, 725, 2101

Rangwala, N., et al. 2011, *ApJ*, 743, 94

Rodríguez-Fernández, N. J., Tafalla, M., Gueth, F., & Bachiller, R. 2010, *A&A*, 516, A98

Sani, E., et al. 2012, *MNRAS*, 424, 1963

Schilke, P., Walmsley, C. M., Pineau des Forets, G., & Flower, D. R. 1997, *A&A*, 321, 293

Schinnerer, E., Eckart, A., Tacconi, L. J., Genzel, R., & Downes, D. 2000, *ApJ*, 533, 850

Snell, R. L., Narayanan, G., Yun, M. S., Heyer, M., Chung, A., Irvine, W. M., Erickson, N. R., & Liu, G. 2011, *AJ*, 141, 38

Spinoglio, L., et al. 2012, *ApJ*, 758, 108

Tacconi, L. J., Gallimore, J. F., Genzel, R., Schinnerer, E., & Downes, D. 1997, *Ap&SS*, 248, 59

Tacconi, L. J., Genzel, R., Blietz, M., Cameron, M., Harris, A. I., & Madden, S. 1994, *ApJL*, 426, L77

- Telesco, C. M. & Decher, R. 1988, ApJ, 334, 573
- Tsai, M., Hwang, C.-Y., Matsushita, S., Baker, A. J., & Espada, D. 2012, ApJ, 746, 129
- Tully, R. B. 1988, Nearby galaxies catalog
- Usero, A., García-Burillo, S., Fuente, A., Martín-Pintado, J., & Rodríguez-Fernández, N. J. 2004, A&A, 419, 897
- van der Werf, P. P., et al. 2010, A&A, 518, L42
- Watanabe, N. & Kouchi, A. 2002, ApJL, 571, L173

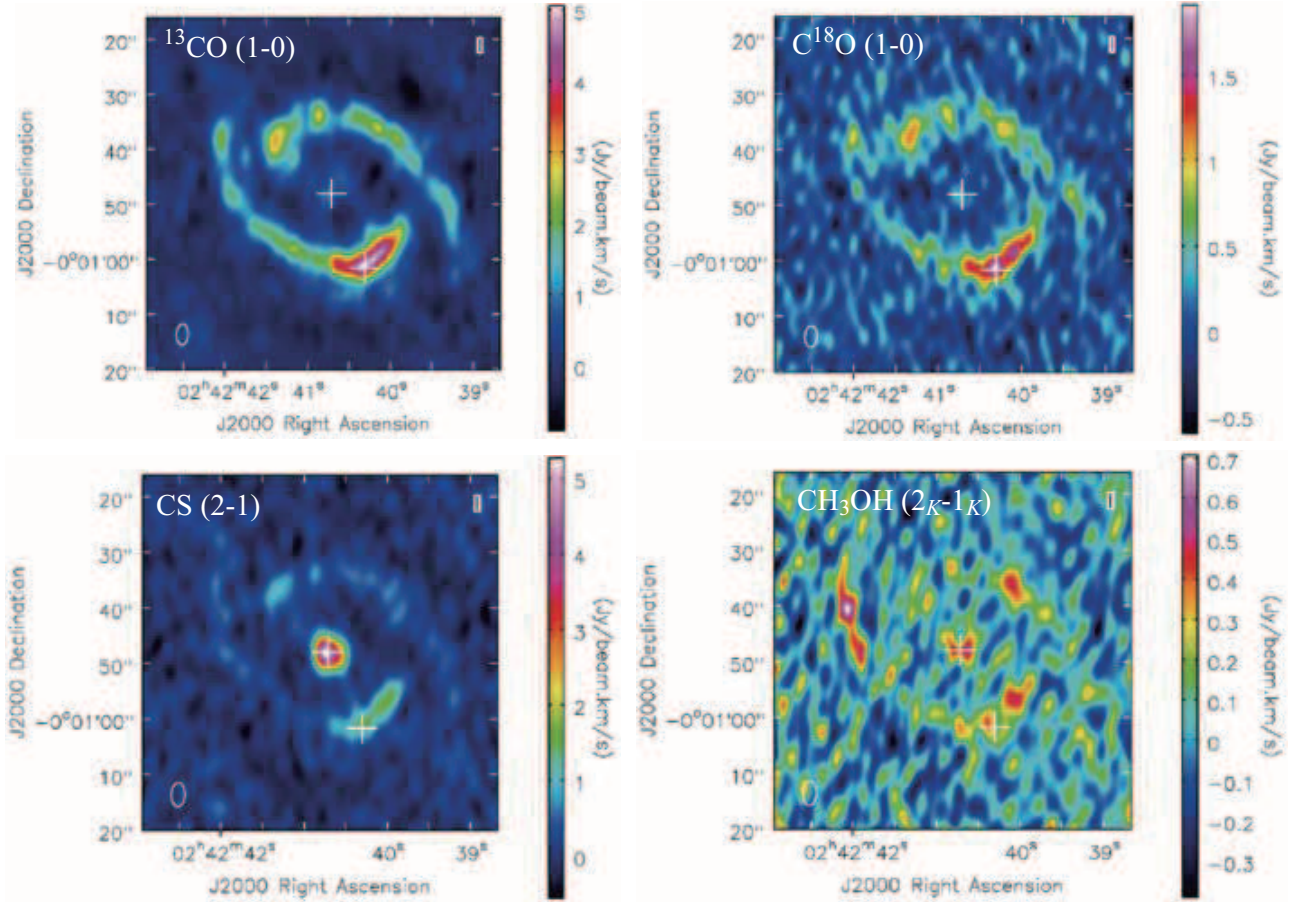


Fig. 1. The images of integrated intensity of $^{13}\text{CO} J = 1-0$, $\text{C}^{18}\text{O} J = 1-0$, $\text{CS} J = 2-1$, and $\text{CH}_3\text{OH} J_K = 2_K-1_K$. The central radio continuum position (RA(J2000.0) = $2^{\text{h}}42^{\text{m}}40^{\text{s}}70912$ and Dec(J2000.0) = $-00^{\circ}00'47''9449$, Gallimore et al. 2004) and the $^{13}\text{CO} J = 3-2$ intensity peak at the southwest position in the starburst ring (RA(J2000.0) = $2^{\text{h}}42^{\text{m}}40^{\text{s}}298$ and Dec(J2000.0) = $-00^{\circ}01'01''638$, Nakajima et al. in preparation) are indicated with white crosses. The beam is shown with an open white ellipse in the bottom-left corner in each image. The primary beam correction is not applied.

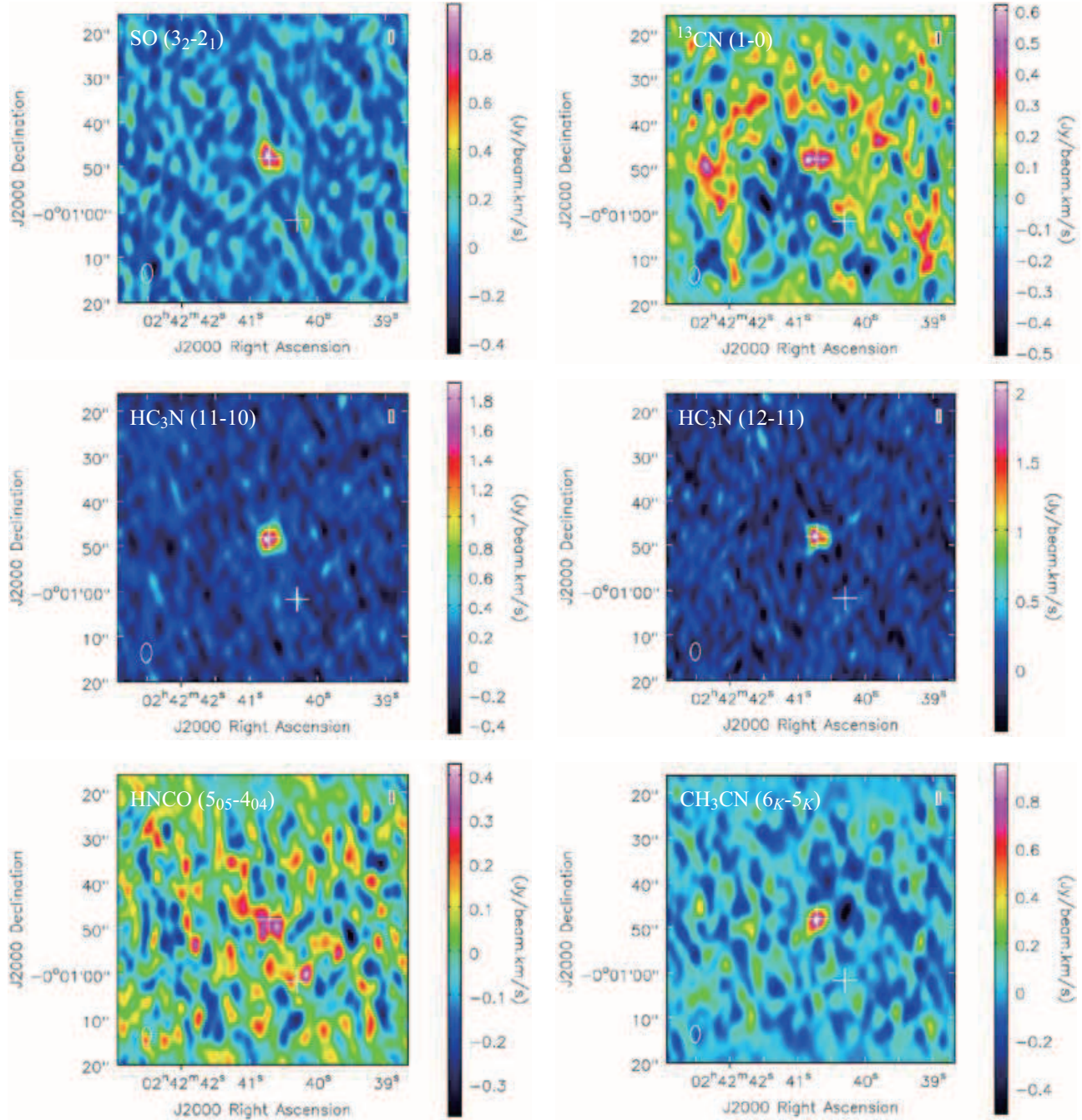


Fig. 2. The images of integrated intensity of SO $J_N = 3_2-2_1$, $^{13}\text{CN } N = 1-0$, $\text{HC}_3\text{N } J = 11-10, 12-11$, and $\text{HNCO } J_{K_a, K_c} = 5_{0,5}-4_{0,4}$, $\text{CH}_3\text{CN } J_K = 6_K-5_K$. The central continuum position and the $^{13}\text{CO } J = 3-2$ intensity peak at the southwest position in the starburst ring are indicated with white crosses (see the caption of figure 1). The beam is shown with an open white ellipse in the bottom-left corner in each image. The primary beam correction is not applied.

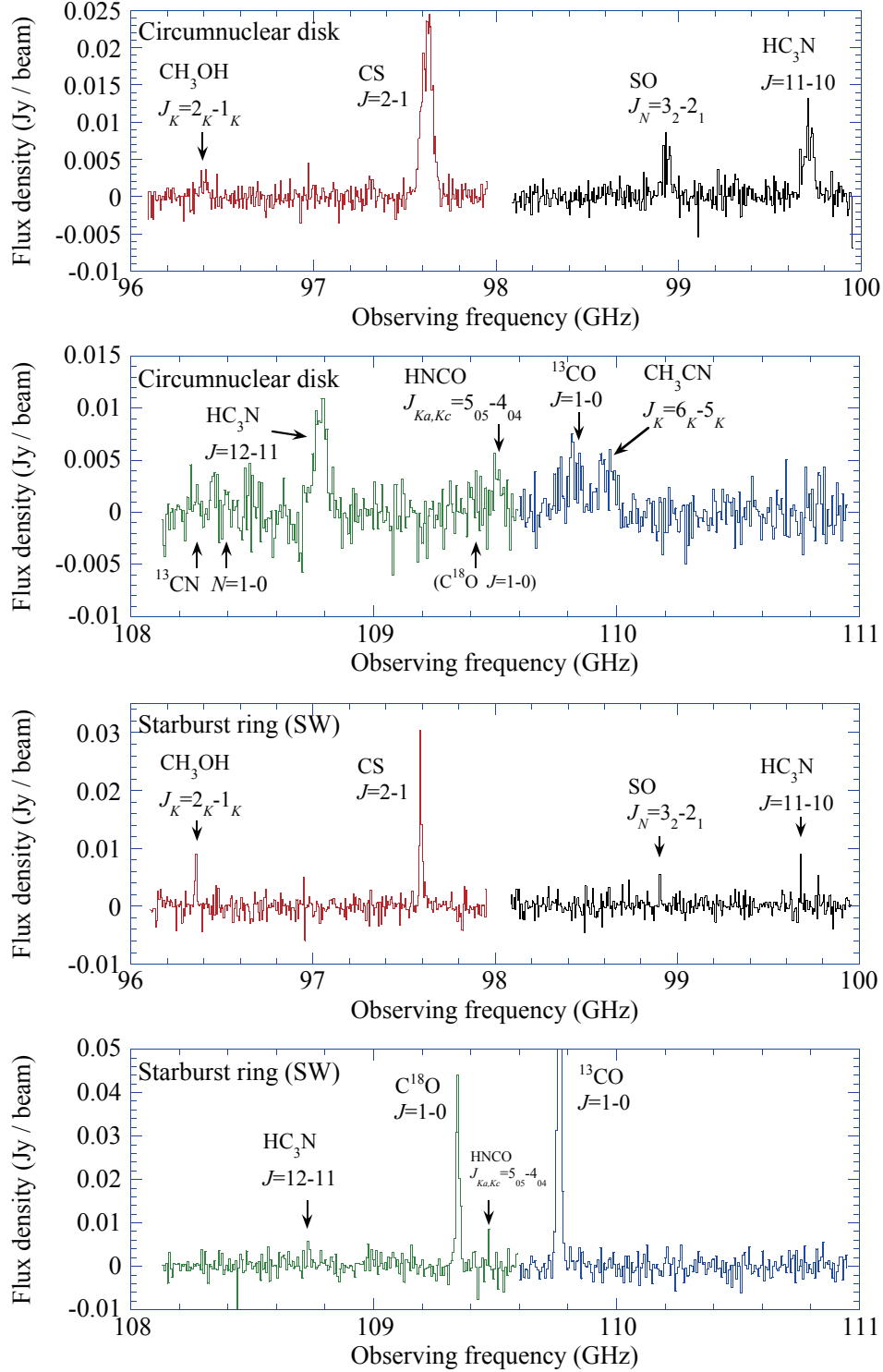


Fig. 3. The spectra are shown at the central continuum position and the ^{13}CO $J = 3-2$ intensity peak at the southwest position in the starburst ring (see the caption of figure 1). The primary beam correction is applied. Different colors of the spectra indicate different spectral windows (spw0, 1, 2, and 3). The frequency is shown as topocentric value, which is a default reference frame of ALMA. It is necessary to shift the frequency corresponding to $V_{\text{LSR}} = 1150 \text{ km s}^{-1}$ to obtain approximate rest frequency.

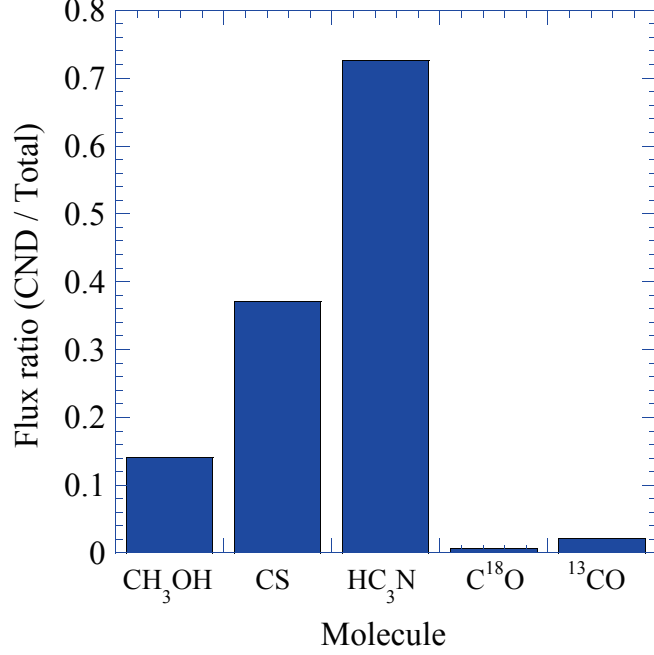


Fig. 4. Flux ratio (circumnuclear disk (CND) / total) is presented for each molecule. For details, see the text (section 3.3).

Table 1. Observational parameters (ALMA Band 3, cycle 0)

Parameter	Value
Date	January 9 and 10, 2012
No. of antennas	16
Configuration	compact
Phase center (Schinnerer et al. 2000)	RA(J2000.0) = 2 ^h 42 ^m 40 ^s .798 Dec(J2000.0) = -00°00'47"938
Bandpass calibrator	J0423-013
Flux calibrator	Callisto
Phase calibrator	J0339-017
Central freq. (GHz) and beam size with its principal axis of each spectral window	97.38 (LSB, spw0), 4''2×2''4 176 deg 99.3875 (LSB, spw1), 4''2×2''2 178 deg 109.4375 (USB, spw2), 3''8×2''2 178 deg 110.4375 (USB, spw3), 3''9×2''1 177 deg
Frequency resolution (kHz)	488
Velocity resolution (km s ⁻¹)	~19.0 at 100 GHz (13 channel binning)
Rms noise (mJy beam ⁻¹)	~1.1–1.7

Table 2: Line parameters of the detected lines

Frequency*	Molecule	Transition	Circumnuclear disk				Starburst ring (SW) [†]				Comment
			Flux density (mJy beam ⁻¹)	V_{LSR} (km s ⁻¹)	FWHM (km s ⁻¹)	$\int \text{flux} dv$ (Jy beam ⁻¹ km s ⁻¹)	Flux density (mJy beam ⁻¹)	V_{LSR} (km s ⁻¹)	FWHM (km s ⁻¹)	$\int \text{flux} dv$ (Jy beam ⁻¹ km s ⁻¹)	
96741.42	CH ₃ OH	$J_K=2_K-1_K$ [‡]	2.3±0.6	1057±20	148±51	0.4±0.1	9.8±1.8	1190±3	29±7	0.31±0.06	
97980.968	CS	$J=2-1$	22.0±0.9	1092±4	209±11	4.9±0.2	29±2	1193±1	37±2	1.13±0.07	
99299.879	SO	$J_N=3_2-2_1$	5.1±0.8	1090±13	166±33	0.9±0.2	6.5±3.5	1188±6	20±12	0.14±0.08	
100076.389	HC ₃ N	$J=11-10$	9.1±0.9	1083±8	178±21	1.7±0.2	9.0±1.6	1190±6	19±6	0.19±0.05	
108657.646	¹³ CN	$N=1-0, J=1/2-1/2$	—	—	—	—	—	—	—	<0.08 (1 σ)	low SN (CND, SB ring)
108780.201	¹³ CN	$N=1-0, J=3/2-1/2$	—	—	—	—	—	—	—	<0.08 (1 σ)	low SN (CND, SB ring)
109173.634	HC ₃ N	$J=12-11$	10.6±0.9	1079±7	171±17	1.9±0.2	5.8±2.0	1216	~30	0.17±0.05	low SN (SB ring)
109782.160	C ¹⁸ O	$J=1-0$	—	—	—	<0.12 (1 σ)	42±2	1191±1	45±3	2.0±0.1	
109905.753	HNCO	$J_{K_a, K_c}=5_{0,5}-4_{0,4}$	3.6±1.1	1078±15	95±37	0.4±0.1	8.5±2.4	1179	17	0.15±0.04	low SN (CND, SB ring)
110201.353	¹³ CO	$J=1-0$	4.0±0.8	1040±24	254±61	1.1±0.2	131±2	1191.2±0.4	44.5±0.9	6.2±0.1	
110383.522	CH ₃ CN	$J_K=6_K-5_K$	4.5±1.0	1169±19	237±70	1.1±0.3	—	—	—	<0.10 (1 σ)	

* Frequency measured in laboratory (Lovas 1992): $J_{K_a, K_c}=2_{0,2}-1_{0,1}A+$ for CH₃OH and $J_K=6_0-5_0$ for CH₃CN.

[†] Values at the peak channel are listed for the HC₃N $J=12-11$ and HNCO $J_{K_a, K_c}=5_{0,5}-4_{0,4}$ transitions, since Gaussian fitting could not be applied. For these transitions, the errors are calculated from the rms noise in the spectra.

[‡] Transitions contributing to this 2_K-1_K group are $J_{K_a, K_c}=2_{-1,2}-1_{-1,1}E$, $2_{0,2}-1_{0,1}A+$, $2_{0,2}-1_{0,1}E$, and $2_{1,1}-1_{1,0}E$.

Table 3. Flux in the circumnuclear disk (CND) and the total flux of each molecule

Molecule	Flux in the CND* (Jy km s ⁻¹)	Total flux† (Jy km s ⁻¹)	Ratio (CND/Total)	Main distribution
CH ₃ OH	1.05±0.03	7.4±0.2	0.141±0.005	CND & starburst ring
CS	10.4±0.3	28.0±0.5	0.37±0.01	CND & starburst ring
SO	1.78±0.05	—‡	—	CND
HC ₃ N <i>J</i> =11–10	3.7±0.1	—‡	—	CND
HC ₃ N <i>J</i> =12–11	3.3±0.1	4.6±0.3	0.73±0.06	CND
¹³ CN	1.55±0.05	—‡	—	(at least) CND
C ¹⁸ O	0.34±0.03	48.0±0.5	0.0063±0.0006	starburst ring
HNCO	1.27±0.03	—‡	—	(at least) CND
¹³ CO	3.07±0.07	143±1	0.0217±0.0005	starburst ring
CH ₃ CN	1.61±0.06	—‡	—	CND

* Flux within the circle with the diameter of 10".

† Flux within the circle with the diameter of 55".

‡ In the case of low signal-to-noise ratio, it is difficult to obtain a reliable flux of the relatively wide area of 55" diameter. For details, see the text (section 3.3).

Table 4. Classification of molecular distributions in the circumnuclear disk (CND) and the starburst ring

Category and Molecule
1. Molecules concentrated in the CND
1–1. Distributed both in the east and west knots ¹³ CN (<i>N</i> = 1–0)*, HNCO (<i>J</i> _{<i>K</i>_a,<i>K</i>_c} = 5 _{0,5} –4 _{0,4})*†, CN (<i>N</i> = 3–2) , CS (<i>J</i> = 7–6)
1–2. Distributed in the center SO (<i>J</i> _{<i>N</i>} = 3 ₂ –2 ₁)†, SiO (<i>J</i> = 2–1)‡, HC ₃ N (<i>J</i> = 11–10, 12–11)†, CH ₃ CN (<i>J</i> _{<i>K</i>} = 6 _{<i>K</i>} –5 _{<i>K</i>})
2. Molecules distributed both in the CND and the starburst ring
2–1. Distributed both in the east and west knots in the CND CH ₃ OH (<i>J</i> _{<i>K</i>} = 2 _{<i>K</i>} –1 _{<i>K</i>}), ¹³ CO (<i>J</i> = 3–2)
2–2. Distributed in the center in the CND CS (<i>J</i> = 2–1), HCN (<i>J</i> = 1–0) [§] , HCO ⁺ (<i>J</i> = 1–0) [§]
3. Molecules distributed mainly in the starburst ring. ¹³ CO (<i>J</i> = 1–0), C ¹⁸ O (<i>J</i> = 1–0, 3–2)

* Note that the signal-to-noise ratio is not high.

† Relatively small portion of the flux is detected in the southwestern part of the starburst ring (see figure 3).

‡ Based on García-Burillo et al. (2010)

§ Based on Jackson et al. (1993), Tacconi et al. (1994), and Kohno et al. (2008)

^{||} See Nakajima et al. in preparation.